ISAS - INTERNATIONAL SCHOOL
FOR ADVANCED STUDIES

Schottky Barrier
in
Al/GaAs junctions

Thesis submitted for the degree of

"Magister Philosophiæ"

CANDIDATE

Alice Ruini

SUPERVISORS

Prof. Raffaele Resta

Prof. Stefano Baroni

October 1995

SISSA - SCUOLA
INTERNAZIONALE
SUPERIORE
STUDI AVANZATI
TRIESTE
Strada Costiera 11

TRIESTE

SISSA ISAS
SCUOLA INTERNAZIONALE SUPERIORE DI STUDI AVANZATI
INTERNATIONAL SCHOOL FOR ADVANCED STUDIES

Schottky Barrier in Al/GaAs junctions

Thesis submitted for the degree of

"Magister Philosophiæ"

CANDIDATE

Alice Ruini

SUPERVISORS

Prof. Raffaele Resta

Prof. Stefano Baroni

October 1995

Table of Contents

1 Introduction

During the past twenty years, components based on metal-semiconductor junctions, also called Schottky Barrier (SB) junctions, have been increasingly used in microelectronics, and research activity has continued with the aim of obtaining a full understanding of the physics of interfacial barrier formation and of current transport across the interface.

In particular, the SB height is the fundamental parameter for characterizing the electronic properties of related devices.

Experimentally it has been found that the barrier height depends on the semiconductor and is generally only weakly sensitive to the metal: the Fermi level is therefore said to be *pinned* within the semiconductor gap for a number of metal-semiconductor interfaces. A clear understanding of the origin of this behaviour is still lacking, even if a large number of models has been proposed. In particular we can distinguish two classes of models: the first one attributes the *pinning* effect to the existence of an intrinsic neutrality level in the semiconductor, while the second one refers to extrinsic gap states induced by interfacial defects.

The SB problem is a really messy one because of uncertainties in the microscopic structure and chemistry of the interface, as well as because of the difficulty of performing reliable spectroscopic measurements on the semiconductor in the presence of a metal. Moreover, it turns out to be difficult to choose one class of models simply by comparing theoretically

predicted barrier heights with experiments because both of them give similar predictions from a quantitative point of view, and mostly in agreement with experimental findings.

In this complicated scenario, the most valuable contribution of a theoretical, parameter-free calculation can be a qualitative understanding of mechanisms which determine the *pinning*. There have been relatively few papers of good computational quality on the Schottky barrier problem. The Al/GaAs system, which is our main interest, has been studied in Refs. [1] [2] [3]. Typically, these papers report the calculated value of the barrier, and some results on charge distributions and local density of states. However, the problem of the pinning and of the relevant mechanism which possibly produces it is even not addressed. Very recently a (still unpublished) work [4] has demonstrated that the pinning exists and is intrinsic. Some very interesting transitivity relationships have also been demonstrated to hold within the (fairly small) computational error. This important work has left many intriguing questions open; in particular the physical mechanism accounting for the pinning and for the transitivity has still to be identified.

In the present work, we build upon the previous findings of ref. [4] in order to check their robustness (under change in growth direction, strain etc.). Our aim is—to start with—producing a much larger database, in order hopefully to detect which are the most relevant features affecting the intriguing phenomenon which is computationally measured. A theoretical investigation (based on self-consistent, first-principles calculations within the local-density functional approximation) of structural and electronic properties of metal-semiconductor interfaces is therefore presented here in order to determine whether Schottky barrier on ideal (e.g. free from defects), unreconstructed interfaces could give rise to the observed Fermi-level pinning for Al/GaAs interfaces.

Ab-initio calculations allow to study ideal interfaces (hardly obtainable in practice) and therefore to "isolate" the most relevant contributions to the *pinning* effect. In particular, as

a first step, it is interesting to establish whether the *pinning* really occurs, how accurately it can be evaluated, and which are the consequences of different conditions on it.

In Chapter 1 the main theoretical models for SB systems are briefly reviewed (for a more detailed discussion of this topic we remind to monographies [5], [6], [7]) and some recent experimental findings are presented. In Chapter 2 we describe the theoretical tools upon which our calculations are based, the geometric modelizations of Al/GaAs junctions and the way of calculating the SB height in our theoretical, *ab initio* framework. Our results, concerning bulk properties of GaAs and Al and mostly SB height determination for (001)Al/GaAs and (110)Al/GaAs junctions are finally presented in Chapter 3, whose last paragraph is devoted to conclusions and perspectives for future work.

2 Schottky Barrier: a field in progress

The basic mechanisms involved in the formation of SB at the metal/semiconductor interface are not yet well understood. The complex features of semiconductor surfaces and interfaces (such as surface relaxation, surface stoichiometry, lattice mismatch and disordering, chemical reaction, interdiffusion, exchange of atoms, presence of defects and metal-induced gap states, etc) make this problem really a difficult one.

2.1 Model theories

In 1938 Schottky explained the rectifying property of metal-semiconductor junctions through a space-charge layer on the semiconductor side of the contact which is depleted of mobile majority carriers. The current of electrons (holes) through the junction is caused by the energy difference between the Fermi level and the bottom (top) of the conduction (valence) band, when the semiconductor is n-doped (p-doped). The sum of the p-barrier and the n-barrier always equals the semiconductor gap.

In their model [8], Mott and Schottky identified the barrier height with the difference between the metal work function Φ_m and the semiconductor electronic affinity χ_s, so we

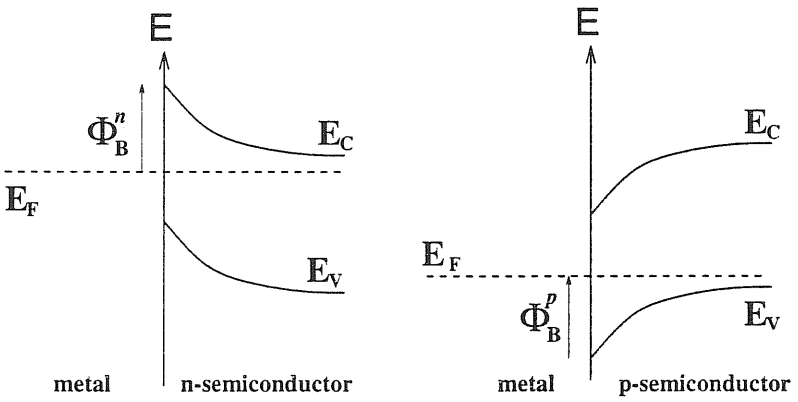

Figure 1.1: Usual schematic representation of the barrier. The band-bending due to semiconductor doping occurs typically at distances of the order of a few hundreds of Å and can be therefore neglected in our atomic-scale study of the region very near to the interface.

get the Schottky-Mott equations:

$$\Phi_B^n = \Phi_m - \chi_s \tag{1.1}$$

$$\Phi_B^p = E_g - \Phi_m + \chi_s = E_g - \Phi_B^n$$

where E_g is the semiconductor gap.

Experience shows that these equations cannot be verified because, in general, the SB height shows typical variations from one metal to the other of the order of 0.2 eV, whereas the range of variation of the work function over different metals is of some eV. Moreover, the metal work function and the semiconductor affinity are not well-defined quantities, because, in general, they depend on the surface across which the electron is extracted.

To overcome the difficulties involved in such a model (characterized by absence of interface-specific phenomena), Bardeen [9] suggested the preponderant role of interface states, i.e. of an interface dipole created by a charge transfer.

After that, virtually all other subsequent workers in the SB field agree that the Fermi-level pinning is caused by electronic states in the band gap, and the only controversial issue is the nature and the origin of these states. We can distinguish two different classes of models.

- The first one is based on intrinsic properties of the semiconductor and suggests that it is possible for the wave functions of those electrons in the metal with energies corresponding to the forbidden gap in the semiconductor to penetrate into the semiconductor in the form of exponentially damped evanescent waves [10]. This represents a transfer of charge from the metal to the semiconductor and the states so arising induced by the presence of the metal (*metal induced gap states*, or MIGS) might dominate the mechanism of Fermi level pinning.

- The second one is instead based on extrinsic interface properties and attributes the pinning to some gap states provided by the formation of interfacial defects. Wieder [11] and Spicer [12], for example, suggest that point defects might occur as a result of the energy released during interface formation.

  Freeouf and Woodall [13] propose to replace the metal work function with an effective one; for the III-V semiconductors they suppose the existence of microscopic anion pack at the interface created during the interface formation and modifying the semiconductor electron affinity.

At present time, it has not been established in a definitive way which picture is the right one.

On one hand an experimental evidence of MIGS is still lacking and the approach underlying this model has been questioned because of the simplicistic treatment of surface structure [14].

On the other hand some recent work [15] indicates that the density of defects necessary

for Fermi level pinning may be much higher than the one known to exist at interfaces. Moreover, if SB heights are determined by Fermi level pinning associated with defects, then they should be unrelated to heterojunction lineups (in fact, at device quality heterojunctions there are very few defects); but the fact that band lineups and barrier heights are so closely connected experimentally argues strongly for a theoretical approach which deals with both of these on a unified footing and gives the relationship between SB and band lineup as a natural result.

Among the models belonging to the first class, it is important to mention the Tersoff's one [16]. The basic idea underlying this approach is to introduce a neutrality level for the semiconductor, playing a role similar to the one of the Fermi level of the metal. The MIGS, corresponding to the queues of the metal wave functions inside the semiconductor, create the dipole needed to align the neutrality and the Fermi level; the metallic screening created by these states tends to align the two levels, so that the local charge neutrality is mantained. This condition allows to define the position of the canonic level E_B of the semiconductor, imposing that a filling of MIGS until this level assures the local charge neutrality [16].

Tersoff extended this model also to heterojunctions between semiconductors, concluding that the energies E_B of both semiconductors have to be nearly aligned, because the screening in the semiconductor should be similar to the one in the metal, owing to the big dielectric constants of the semiconductors ($\epsilon > 10$).

Following Tersoff's model, the mechanism governing the band alignment for a semiconductor-semiconductor heterojunction is the same as for a metal-semiconductor junction, since it forces the reference energy levels of both materials to be aligned and this alignment condition is transitive. Moreover, if the same mechanism is responsible for the band line-up in both types of junctions, then the difference between n- or p-SB of a metal M with two semiconductors A and B should equal the valence band discontinuity (VBO) or the conduction

band discontinuity (CBO) for the A/B heterojunction:

$$\Phi_B^n(M/A) - \Phi_B^n(M/B) = CBO(A/B) \qquad (1.2)$$
$$\Phi_B^p(M/A) - \Phi_B^p(M/B) = VBO(A/B)$$

Besides, Φ_B should be metal-independent. Equation 1.2 is often referred to as transitivity rule.

The Tersoff's model is appealing because of its simplicity, but it lacks of a formal physical basis. Particularly in the case of semiconductor heterojunctions, where our theoretical understanding is much better, it has been proved that the Tersoff's model is only a rough guideline, accurate no better than 0.3 eV.

1.2 Experimental findings

During recent years, the application of modern experimental techniques has shown clearly that interfaces formed between metals and semiconductors are highly dependent on the preparation procedure. In order to understand the fundamental physics of contacts to semiconductors the most important studies are those where metals have been deposited onto atomically clean and ordered surfaces and only in a few cases (e.g. aluminum on gallium arsenide) it has been possible to prepare epitaxial single crystal contacts with virtually perfect interfaces to the semiconductor. Nonetheless, even in such a case of epitaxial growth, Al atoms have been demonstrated to be highly mobile both on GaAs(110) and on GaAs(001) surfaces and chemical reactions have been detected [17].

A wide range of surface-science techniques has been applied to study the microscopic interactions and Schottky barrier formation for metals deposited on clean III-V semiconductors. Extensive studies of Schottky barrier heights for thick metal layers on III-V semiconductors have been carried out using I/V, C/V, and photoresponse (internal photoemission,

IPE) methods, the samples being mostly obtained growing the metal on a semiconductor substrate with *Molecular Beam Epitaxy* (MBE) technique.

External perturbations, such as pression, temperature or compositional variation, produce a shift of band levels with respect to the level responsible for the pinning, so that they can give useful informations in order to determine the dominant mechanism in Fermi level pinning. Some measurements of SB variation with pressure, temperature and semiconductor composition have been in fact recently performed [18] [19] on (001)-Al/$Ga_{1-x}Al_xAs$ junctions

In particular this experimental study shows that, with composition variation, the p(n)-barrier follows the band discontinuity VBO (CBO) of $Ga_{1-x}Al_xAs$ within the experimental precision ($\sim$ 0.1 eV), according to the transitivity rule (1.2).

2 Theoretical backgrounds

2.1 Ab-initio self-consistent calculations

In order to obtain a description of the actual electron distribution at the interface, one has to perform calculations in which the electrons are allowed to readjust to the specific environment determined by the different ionic species at the interface.

Density-Functional Theory (DFT) provides a fundamental theoretical framework to face this problem with *ab initio* calculations.

In the spirit of the Born Oppenheimer approximation, the electronic degrees of freedom can be decoupled from the ionic ones. Ionic cores behave as classical particles and, given a certain ionic configuration, their potential energy is given by the ground state energy of the electrons which constitute a quantum many-body system. This approach relies on the large mass difference between ions and electrons, which implies that electrons remain very close to their ground state configuration while the ions move. For this reason, the knowledge of the electronic ground state allows a complete description of the properties of the system. DFT provides a theoretical tool to calculate ground state properties of a quantum many-electron system without solving the many-body Schrödinger equation, which would be an impossible task due to the large number of the degrees of freedom involved in the calculation. A central result [20] of DFT is that the ground state energy of a system of interacting electrons can

be obtained, at least in principle, by minimizing the functional:

$$E[n] = F[n] + \int V(\mathbf{r})n(\mathbf{r})d(\mathbf{r}), \tag{2.1}$$

where $F[n]$ is a universal function of the electronic density (*i.e.* it is independent on $V(\mathbf{r})$), and $V(\mathbf{r})$ is the external potential in which the electrons move, that in crystals corresponds to the potential generated by the ionic cores. The form of $F[n]$ is in general unknown, and in order to apply this theory in actual calculations, Kohn and Sham proposed for this functional the following *ansatz*:

$$F[n(\mathbf{r})] = T_0[n(\mathbf{r})] + \frac{1}{2}\int \frac{n(\mathbf{r})n(\mathbf{r}')}{|\mathbf{r}-\mathbf{r}'|}d\mathbf{r}d\mathbf{r}' + E_{xc}[n(\mathbf{r})]. \tag{2.2}$$

$F[n]$ consists of a term ($T_0[n]$) due to the kinetic energy of a noninteracting electron system with density $n(\mathbf{r})$, and of a Hartree term, corresponding to the classical electromagnetic interaction between the electrons (Hartree units are used throughout the discussion). Equation (2.2) defines the exchange and correlation energy $E_{xc}[n]$ as the difference between the unknown functional $F[n]$ and the known term in its r.h.s.. Minimizing the above functional with the constraint $\int n(\mathbf{r})d\mathbf{r} = N$, we obtain a set of self-consistent equations [21]:

$$\underbrace{\left[-\frac{\nabla^2}{2} + V_{SCF}(\mathbf{r})\right]}_{H_{KS}}\psi_i(\mathbf{r}) = \epsilon_i\psi_i(\mathbf{r}) \tag{2.3}$$

$$V_{SCF} = V(\mathbf{r}) + \int \frac{n(\mathbf{r}')}{|\mathbf{r}-\mathbf{r}'|}d\mathbf{r}' + v_{xc}(\mathbf{r}), \tag{2.4}$$

$$n(\mathbf{r}) = \sum_i |\psi_i(\mathbf{r})|^2\,\theta(\epsilon_i - \epsilon_f). \tag{2.5}$$

These are the well-known Kohn-Sham (KS) equations, where the Fermi energy ϵ_f is defined by the constraint on the number of electrons in the system and $v_{xc}(\mathbf{r}) = \delta E_{xc}[n]/\delta n(\mathbf{r})$ is the exchange-correlation potential. Due to this unknown term, the Kohn and Sham equations are of no practical use, unless an approximation for v_{xc} is specified. The most used approximation in practical calculations is the so called *Local Density Approximation*

(LDA), in which the exchange-correlation energy is taken as a local function of the density itself: $E_{xc}[n] = \int n(\mathbf{r})\epsilon_{xc}(n(\mathbf{r}))d\mathbf{r}$, where $\epsilon_{xc}(n(\mathbf{r}))$ is the exchange-correlation energy per particle of the homogeneous electron gas at a density equal to the local density $n(\mathbf{r})$. In this way the potential v_{xc} is given by:

$$v_{xc}(\mathbf{r}) = \mu_{xc}(n(\mathbf{r})) = \frac{d}{dn}[n\epsilon_{xc}(n)]. \tag{2.6}$$

From the solution of the KS equations we can so get, through equation (2.5), the knowledge of the electron-density distribution, which is the quantity we are interested in (as will be discussed in Section 2.3).

To solve in practice the KS equations, one can write the KS orbitals in terms of a suitable finite basis set. When the plane-wave (PW) basis set is chosen, taking advantage of the translational invariance and the resulting Bloch theorem, the KS orbitals can be expanded as

$$\psi_i(\mathbf{r}) = \psi_{n,\mathbf{k}}(\mathbf{r}) = \sum_{\mathbf{G}} e^{i(\mathbf{k}+\mathbf{G})\mathbf{r}} c_{n\mathbf{k}}(\mathbf{G}), \tag{2.7}$$

where $\mathbf{k}$ belongs to the first Brillouin Zone (BZ) of the crystal, $\mathbf{G}$ is a reciprocal lattice vector, and n is the band index. The dimension of the PW basis set is determined by fixing the kinetic energy cutoff, E_{cut}, through the condition:

$$|\mathbf{k} + \mathbf{G}|^2 \leq E_{cut}. \tag{2.8}$$

The choice of a PW basis has the advantage that the matrix elements of the Hamiltonian in Eq. 2.3 are particularly simple and that the accuracy of the expansion can be easily checked and systematically improved by increasing the value of E_{cut}. Furthermore, PW's are independent of the structure of the crystal. In order to obtain an accurate description of the system with a reasonably small number of PW's the core electrons are frozen in the atomic configuration around the nuclei, and only the chemically active valence electrons are treated explicitly. To this end, a smooth angular-momentum-dependent *pseudopotential* is

then introduced to describe the interaction between valence electrons and ionic cores (nuclei + core electrons). There are many different schemes to generate ionic pseudopotentials from first-principles (see for example [22][23]). Basically, all of them satisfy the following requirements: (*i*) the lowest pseudo-energy levels are equal to the valence all-electron energies; (*ii*) each pseudo-wave function coincides with the corresponding all-electron one outside a properly chosen core radius; (*iii*) as a consequence of (*ii*), the real and pseudo charge inside the core radius agree for each valence state. This last condition is called *norm conservation*, and ensures the transferability of the pseudopotential to different chemical environments. The accuracy of the results obtained with *norm-conserving* pseudopotentials is comparable with those from all-electron calculations [24, 25].

In our particular case we are interested in the study of the electronic properties of interfaces and these are actually described by periodically repeated supercells, containing two complementary interfaces; it is important to stress that supercells allow in fact a reciprocal space formulation of the problem and the use of PW's, otherwise not possible because of the loss of translational symmetry. The isolated interface configuration is then well represented, provided that the two adjacent interfaces are sufficiently spatially separated in order to not interact. This is verified *a posteriori*, by examining the charge density and the Hartree potential in the regions far from the interface and showing that they are identical to those of the bulk metal and of the bulk semiconductor.

3.2 Geometric modelization for (001)-Al/GaAs and (110)-Al/GaAs junctions

GaAs and AlAs semiconductors crystallize in zincblende structure; moreover they are experimentally nearly lattice matched, in fact they have the same lattice parameter within

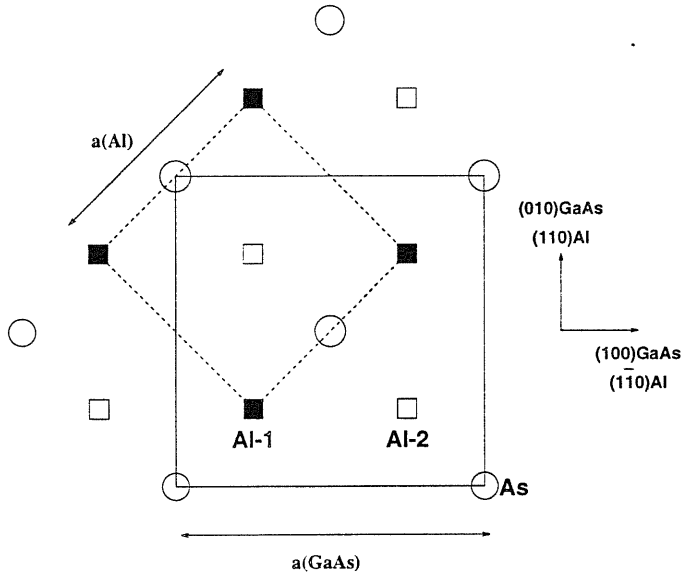

Figure 3.1: Top-view for the (001)Al/GaAs supercell.

0.2% . Aluminum is instead a FCC-metal. Two directions of growth for aluminum on a GaAs-substrate will be considered in this work, i.e. along both (001)- and (110)-direction.

- Our first case study is the (001) direction of growth. In this case, structurally very simple and often realized in experiments, the (001) axes of Al and GaAs are parallel. Since the Al and GaAs lattice constants approximately satisfy $a_{\mathrm{GaAs}} \approx \sqrt{2}a_{\mathrm{Al}}$, Al can be grown on a GaAs(001) substrate if it is rotated 45° about its (001) axis, so that the Al (110) direction points along the GaAs (100) one (see Fig. 3.1).

  As we already pointed out, in order to use periodic boundary conditions in the calculations, the Al/GaAs(001) junction is modeled as a superlattice. It is also important to stress that, compared to band offset calculations at semiconductor-semiconductor heterojunctions, where a 6+6 superlattice (i.e. $(GaAs)_3(AlAs)_3$) is more than sufficient to extract accurate band offset [26], Schottky barrier calculations require much longer supercells because of the presence of the MIGS, whose charge decays evanescently in the semiconductor region.

Our semiconductor slab is made of 13 atomic layers (six Ga layers and seven Al layers), and is therefore As-terminated on both sides (this choice is dictated by the higher stability of the As-terminated GaAs(001) surface with respect to the Ga-terminated one). Our metallic slab is made of 7 layers of Al (each contributing two atoms per supercell). The supercell contains therefore 27 atoms altogether, and has in it two equivalent interfaces with Al-As bonds.

- Our second case study is the (110) direction of growth. Even this case is structurally very simple and has often been realized in experiments. In this case the interfaces are built by making the (110) planes in the semiconductor parallel to those in the metal; the lattice-matching condition is fulfilled provided that the Al(110) surface is rotated by 90° about the [110]-direction. As in the (001)-case, the calculations employ again the slab geometry and the supercell contains seven layers of GaAs and seven layers of Al atoms (contributing two atoms per layer), so that we totally deal with a supercell of 28 atoms and two equivalent interfaces (as shown in Fig. 3.2). Our (001) and (110) supercells have a comparable number of atoms, and therefore are almost equally computer demanding. However, the thickness of the former is greater (by a factor of $\sqrt{2}$), thus better approximating the isolated-interface limit.

3.3 Method for Schottky barrier height determination

We determine Schottky barrier heights within the present LDA calculations as follows: the p-type barrier height is the difference between the metal Fermi level and the semiconductor valence maximum at a distance across the interface which is small compared to any band-bending length (typically hundreds of lattice spacings) but larger than the 4-5 monolayer distance on either side of the interface where the constituents have a charge density (elec-

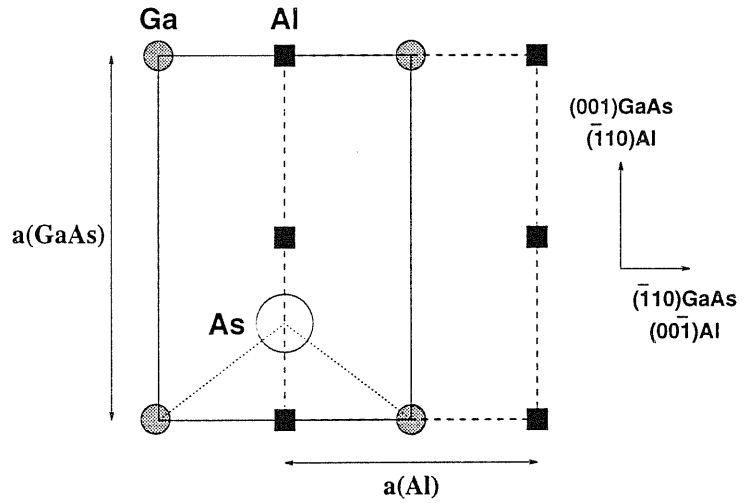

Figure 3.2: Top-view for the (110)Al/GaAs supercell.

tronic and nuclear) that is not identical to that in their respective bulk materials; so, we can write:

$$\Phi_B^p = E_F - E_v. \tag{3.9}$$

This equation can be expressed as:

$$\begin{aligned}\Phi_B^p &= [E_F - < V >]_m - [E_v - < V >]_{sc} \\ &+[< V >_m - < V >_{sc}]_{IF} \\ &= \Delta E_F - \Delta E_v + \Delta V.\end{aligned} \tag{3.10}$$

The first term on the right-hand side is the Fermi energy in the bulk metal with respect to the average potential $< V >= V_m(\mathbf{G} = 0)$ in that material. The second term is the energy of the valence-band edge in the bulk semiconductor with respect to its average potential $< V >= V_{sc}(\mathbf{G} = 0)$. The two band-structure terms are bulk properties of the two materials. They have nothing to do with the metal/semiconductor interface, except for the fact that the strain configurations of the constituent materials in the pure bulk forms must be identical to the strain configuration on either side of the interface.

The average potentials $< V >$ are ill-defined quantities, but their difference ΔV is well-defined and can be obtained with a supercell calculation. In fact, the third term in Eq. (3.10) is the interfacial dipole, i.e. the difference in the average potential on either side of the metal-semiconductor interface (at the intermediate length scale defined above). It is simple to argue that ΔV is the sum of two contributions: the first is the Hartree potential discontinuity, while the second is provided by the Coulomb potential discontinuity, due to ionic point charges. Their calculation requires, respectively, the knowledge of electronic charge density $\rho_{\rm el}(\mathbf{r})$ and of ionic charge density $\rho_{\rm ion}(\mathbf{r})$.

The self-consistent calculation of the electronic charge density in the supercell provides the Fourier coefficients $\rho_{\rm el}(\mathbf{G})$ of the electronic charge density:

$$\rho_{\rm el}(\mathbf{r}) = \sum_{\mathbf{G}} \rho_{\rm el}(\mathbf{G}) \exp(i\mathbf{G}\cdot\mathbf{r}). \tag{3.11}$$

Since we work in reciprocal space using PW's, we have chosen to approximate the point-like ionic charge density using very narrow Gaussian functions centered on the atomic positions τ_s:

$$\rho_{\rm ion}(\mathbf{r}) = \sum_{\mathbf{R}} \sum_{s=1}^{N} Z_s \left(\frac{\alpha}{\pi}\right)^{3/2} exp(-\alpha \mid \mathbf{r} - \tau_s - \mathbf{R} \mid^2), \tag{3.12}$$

where τ_s and Z_s represent, respectively, the positions and the charges of the N ions in the supercell at $\mathbf{R}$ and α is such to warrant that the ionic charge density is relevant only in the immediate neighborhood of the atoms and goes rapidly to zero elsewhere. On the other side, α is such that the planar average of the ionic density is correctly reproduced by our one-dimensional truncated Fourier series. The electrostatic energy $\mathrm{V}(\mathbf{r})$ is related to the charge density by the Poisson's equation

$$\nabla^2 \mathrm{V}(\mathbf{r}) = 4\pi e \rho(\mathbf{r}), \tag{3.13}$$

where the charge density ρ is made of an electronic contribution, due to the valence electrons,

and an ionic contribution, due to the ionic cores of positive charge:

$$\rho(\mathbf{r}) = e\,(\rho_{\mathrm{el}}(\mathbf{r}) - \rho_{\mathrm{ion}}(\mathbf{r})). \tag{3.14}$$

The integral of the valence electron density ρ_{el} and of the ionic cores density ρ_{ion} over the supercell volume Ω equals the number of valence electrons N_{el} within the supercell:

$$\int_{\Omega} \rho_{\mathrm{el}}(\mathbf{r})d\mathbf{r} = \int_{\Omega} \rho_{\mathrm{ion}}(\mathbf{r})d\mathbf{r} = N_{\mathrm{el}}, \tag{3.15}$$

and the system is globally neutral. The Poisson's equation is easily solved in reciprocal space

$$\mathrm{V}(\mathbf{G}) = 4\pi e \frac{\rho(\mathbf{G})}{|G|^2}, \tag{3.16}$$

where $\mathbf{G}$ is a vector non vanishing of the reciprocal lattice. The $|\mathbf{G}| = 0$ term is not included because all the energies are calculated with respect to the average electrostatic energy $\mathrm{V}(\mathbf{G} = 0)$, that is set to zero.

We fix the following notation for the Fourier transform of a function f periodic on the supercell Ω:

$$f(\mathbf{G}) = \frac{1}{\Omega}\int_{\Omega} f(\mathbf{r})e^{-i\mathbf{G}\mathbf{r}}d\mathbf{r} \tag{3.17}$$

$$f(\mathbf{r}) = \sum_{\mathbf{G}} f(\mathbf{G})e^{i\mathbf{G}\mathbf{r}}. \tag{3.18}$$

Both the electrostatic energy $\mathrm{V}(\mathbf{r})$ and the density $\rho(\mathbf{r})$, are periodic functions on the supercell that models our interfaces and they oscillate rapidly on the scale of the interatomic bulk distance within the slab. Since we are interested in the macroscopic properties of these quantities, we have to average out the oscillations on the scale of the interatomic bulk distance. This is done in two steps, following reference [27]. First we define the *planar average* $\overline{f}(\mathrm{z})$:

$$\overline{f}(z) = \frac{1}{\Omega_{||}}\int_{||} f(x,y,z)dxdy, \tag{3.19}$$

where f is one of the quantities we are interested in, the density $\rho(\mathbf{r})$ or the electrostatic energy $V(\mathbf{r})$, $\Omega_{||}$ is the area of the supercell in the plane (xy) parallel to the surface and $\mathbf{r}=(x,y,z)$ is a point in the supercell. Second, we define the *macroscopic average* $\overline{\overline{f}}(z)$, as the one-dimensional average of $\overline{f}$ over a period centered at z:

$$\overline{\overline{f}}(z) = \frac{1}{a}\int_{z-\frac{a}{2}}^{z+\frac{a}{2}} \overline{f}(z')dz' = \frac{1}{a}\int \Theta(\frac{a}{2} - |z-z'|)\overline{f}(z')dz', \tag{3.20}$$

where Θ is the step function and a is the interplanar distance in the bulk. This is equivalent to average $f(\mathbf{r})$ over a slab-adapted bulk unit cell centered at the point $\mathbf{r}$, and therefore it corresponds to the usual definition of macroscopic quantities in electrostatics. The planar average of the electrostatic energy can be calculated, using 3.18 and 3.19, as follows:

$$\overline{V}(z) = \sum_{G_z \neq 0} e^{iG_z z} V(\mathbf{G}_{||} = 0, G_z), \tag{3.21}$$

where

$$V(\mathbf{G}_{||} = 0, G_z) = \frac{4\pi e}{G_z^2}\rho(\mathbf{G}_{||} = 0, G_z). \tag{3.22}$$

The ionic contribution to the density ρ is a superposition of gaussian functions centered on the atomic positions τ_s, and its Fourier transform is:

$$\rho_{\text{ion}}(\mathbf{G}_{||} = 0, G_z) = \sum_s \frac{Z_s}{\Omega} e^{-iG_z\tau_{s,z}} e^{-G_z^2/4\alpha}, \tag{3.23}$$

where the sum runs over all the atoms s within the supercell Ω, and Z_s is the valence charge of the atom s.

Moreover, in our particular case, one has to consider that the planar average of the potential $\overline{V}(z)$ has two different microscopic periodicities in the metal (a_m) and in the semiconductor (a_{sc}); so one has to average $\overline{V}(z)$ with a double filtering in order to eliminate the microscopic potential variations within both materials. The macroscopic average of the potential $\overline{\overline{V}}(z)$ can be then written as:

$$\overline{\overline{V}}(z) = \frac{1}{a_m a_{sc}} \int\int \overline{V}(z)\Theta(\frac{a_m}{2} - |z-z'|)\Theta(\frac{a_{sc}}{2} - |z-z''|)dz'dz''$$

$$= \sum_{G_z \neq 0} \overline{\overline{V}}(G_z) e^{iG_z z}, \tag{3.24}$$

where

$$\overline{\overline{V}}(G_z) = \overline{V}(G_z) \frac{sin(G_z a_m/2)}{G_z a_m/2} \frac{sin(G_z a_{sc}/2)}{G_z a_{sc}/2}. \tag{3.25}$$

The discontinuity ΔV is finally obtained by evaluating the difference

$$\Delta V = \overline{\overline{V}}(z_1) - \overline{\overline{V}}(z_2), \tag{3.26}$$

where z_1 identifies a position within the metal, far from the interface, while z_2 identifies a position within the semiconductor, far from the interface.

4 Results

4.1 Bulk properties of GaAs and Al

As a preliminary step towards the study of Al/GaAs junctions, we have analyzed the structural properties both of bulk aluminum and of bulk gallium arsenide. The properties of the unperturbed crystals are studied within the formalism of the Density Functional Theory in the Local Density Approximation, using the plane-wave pseudopotential method. The BZ sampling is performed on a uniform cubic grid in k-space, following the Monkhorst and Pack scheme [28]. Owing to the point symmetry of the lattice only points in the so called irreducible wedge (IW) of the BZ need to be sampled.

The equilibrium structure is determined by minimizing the total energy of the crystal with respect to the lattice parameter a. For this purpose, the values of the total energy calculated with a fixed kinetic-energy cutoff at different lattice parameters have been fitted to a Murnaghan's equation of state:

$$E(\Omega) = \frac{\Omega_0 B_0}{B_0'}\left[\frac{1}{B_0'-1}\left(\frac{\Omega_0}{\Omega}\right)^{B_0'-1} + \frac{\Omega}{\Omega_0}\right] + \text{const}, \tag{4.1}$$

where B_0 is the bulk modulus, B_0' its derivative with respect to the pressure, and $\Omega_0 = a_0^3/4$ the equilibrium volume of the unit cell.

Table 4.1: Errors of the total energy of GaAs bulk due to different energy cutoffs and special point sampling at the experimental lattice constant . The differences are in mRy. The converged value (within $\simeq$ 1 mRy) of the total energy is also reported (in Ry).

E	6 pt.	10 pt.	19 pt.	60 pt.
14 Ry	35.77	34.54	34.46	34.27
18 Ry	11.72	10.40	10.28	10.10
22 Ry	5.36	4.24	4.05	4.01
26 Ry	3.17	2.06	1.88	1.81
30 Ry	1.13	0.25	0.05	(-17.32129)

4.1.1 Gallium arsenide

GaAs is a binary compound semiconductor. belonging to the III-V group.

To describe the interaction between valence electrons and ionic cores, we use both for Ga and for As the norm-conserving pseudopotential of Bachelet, Hamann, and Schlüter [22] in Kleinman-Bylander [29] form (in order to reduce the computational effort) and made ghost-free by Gonze [30].

Table 4.1 shows a convergence study for the total energy of GaAs bulk with respect to the energy cutoff and to special point sampling at the experimental lattice constant (a_0 = 10.68 a.u.). So, the PW basis set used has a kinetic energy cutoff of 26 Ry and the BZ-integration is performed using a uniform (10×10×10) grid (i.e. 19 k-points in the IW). It has also been checked that these parameters are sufficient to obtain accurate results (converged within $\sim$ 1%) for the structural parameters achieved by interpolating Eq. 4.1 , and the outcomes are displayed in tab. 4.2 in comparison with the experimental ones. The discrepancy with the experimental values is 1.9% for the lattice parameter and 1.8% for the bulk modulus.

This agreement is good and comparable with the typical accuracy of LDA calculations for semiconductors.

4.1.2 Aluminum

Crystalline Al is a group IIIA metal and displays a FCC structure.

The pseudopotential used to describe aluminum has been obtained with the method originally proposed by von Barth and Car [31]: for this pseudopotential we checked the absence of ghost-states.

As for all other metals, the main difficulty is in relation with the description of its Fermi surface and the special point technique must be used with care in this case. The BZ integration is in fact performed with the "smearing" technique described in [32], using the Hermite-Gauss smearing function of order $N = 1$. and a smearing width $\sigma = 10$ mRy. As first step, a kinetic-energy cutoff of 22 Ry has been chosen, by imposing a total-energy convergence of the order of 1 mRy and verifying that it was enough to assure the structural parameters to be converged within 1% . Convergence with respect to BZ sampling and smearing width σ has been further controlled, keeping in mind that the smaller is the value of the smearing width σ, the finer is the mesh needed to achieve convergence with respect to the number of sampling k-points. For $\sigma = 10$ mRy a mesh of 85 points (corresponding to a (18×18×18) grid) in the IW is enough to assure a satisfactory convergence of the calculated quantities (i.e. both of the total energy and of the structural parameters). The values so obtained are shown in Tab. 4.2, compared with the corresponding experimental ones.

4.2 Unperturbed (001)Al/GaAs junction

As a first step we performed our first-principle study with the assumption of an interfacial geometry obtained simply by layering a truncated bulk piece of metal onto a truncated bulk

Table 4.2: Lattice parameters and bulk modulus for GaAs and Al.

	$a_0^{th}(a.u.)$	$a_0^{exp}(a.u.)$	perc.diff.	$B_0^{th}(GPa)$	$B_0^{exp}(Gpa)$	perc.diff.
GaAs	10.48	10.68	1.9%	76.8	75.5	1.8%
Al	7.48	7.64	2.1%	82.5	79.3	4.0%

piece of semiconductor. We also make the approximation of considering a fake aluminum, which is perfectly lattice-matching with the equilibrium lattice parameter of bulk-GaAs, so that it keeps its FCC structure in the supercell, and we choose to take as distance between the last As-plane and the first Al-plane the average plane spacing in Al region and in GaAs region.

The theoretical lattice-mismatching is indeed 0.93 %, and the experimental one is 1.16 %. Therefore the above assumptions are not justified if the aim is to compare the theoretical results with the experiment. But the aim of the present work is different. We want to investigate the pinning—and the physical mechanisms which determine it—at the most fundamental level, neglecting for the time being all the complications and the corrections which we believe are less relevant to the basic phenomenon.

We have performed the BZ integration using a uniform (8×8×1) grid, which turns out to have approximatively the same density as the grid used for bulk calculations.

The top of the valence band for GaAs, ΔE_v = 5.17 eV, has been calculated with a cut-off energy E_{cut} = 26 Ry and a Monkhorst-Pack (10×10×10)-grid.. The Fermi level for our fake Al, ΔE_F = 8.65 eV, has been obtained with the same cut-off energy and with a more dense grid (16x16x16).

The 13+7-supercell described in section 2.2 allows us to obtain the discontinuity ΔV both of the Hartree potential and of the ionic one. It is clear from figure 4.1 that the electronic

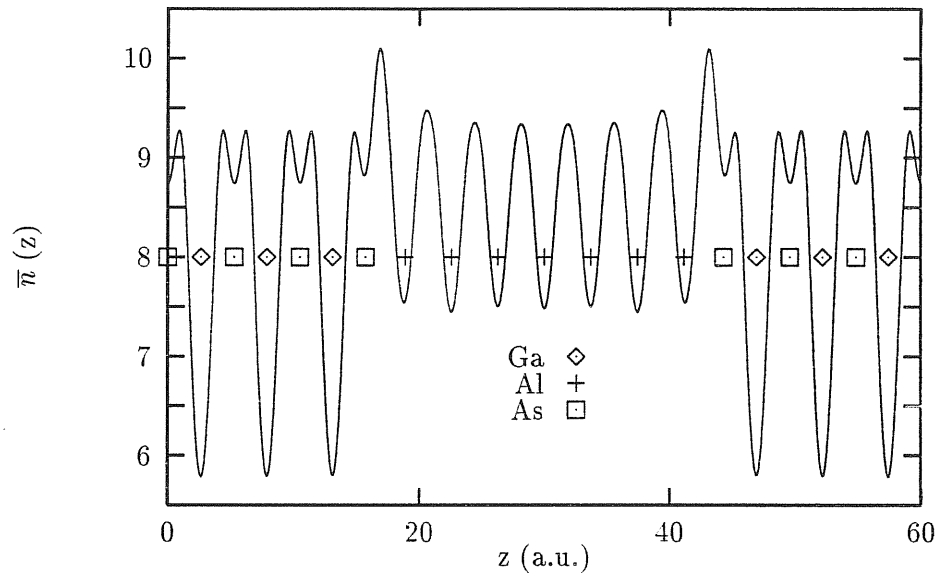

Figure 4.1: Planar average of the electronic charge density for the (001)Al/GaAs supercell.

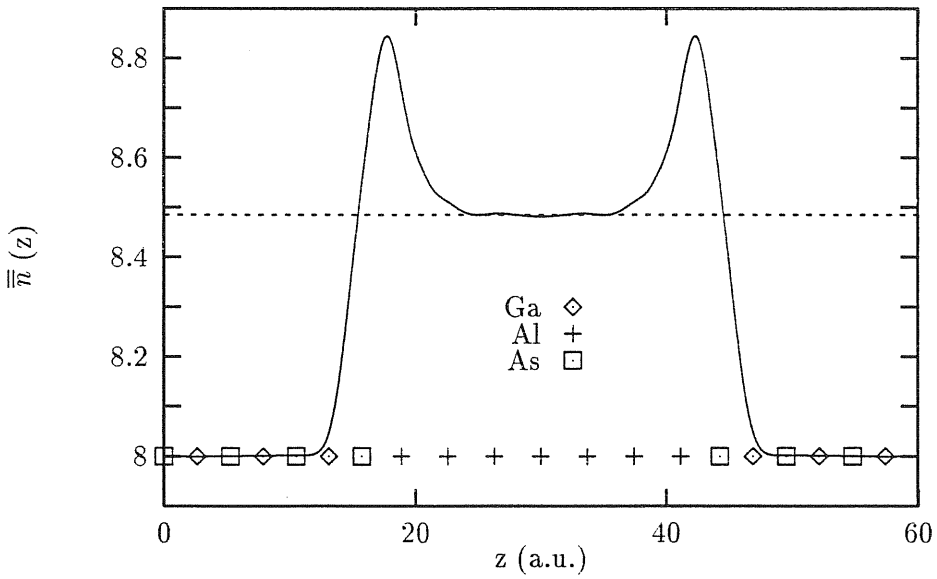

Figure 4.2: Macroscopic average of the electronic charge density for the (001)Al/GaAs supercell.

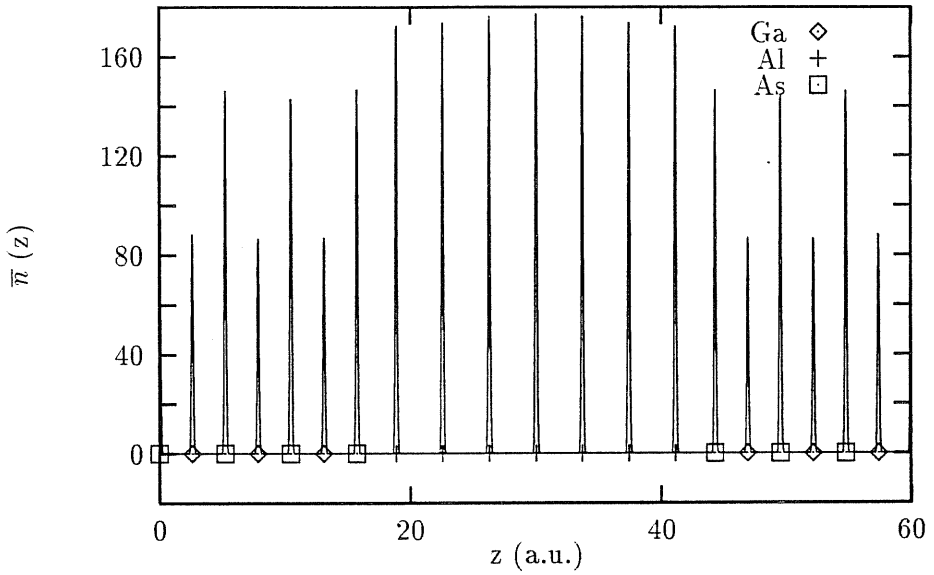

Figure 4.3: Planar average of the ionic charge density for the (001)Al/GaAs supercell.

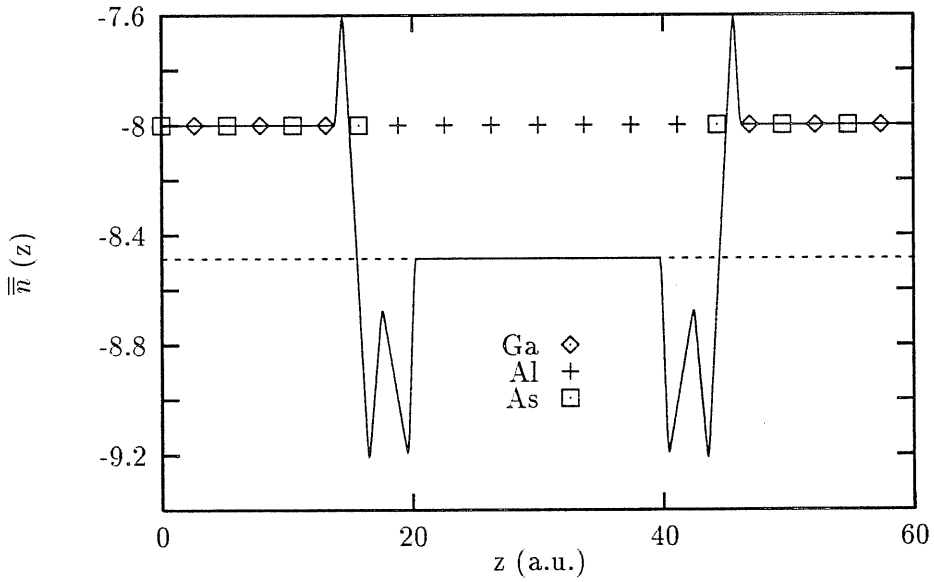

Figure 4.4: Macroscopic average of the ionic charge density for the (001)Al/GaAs supercell.

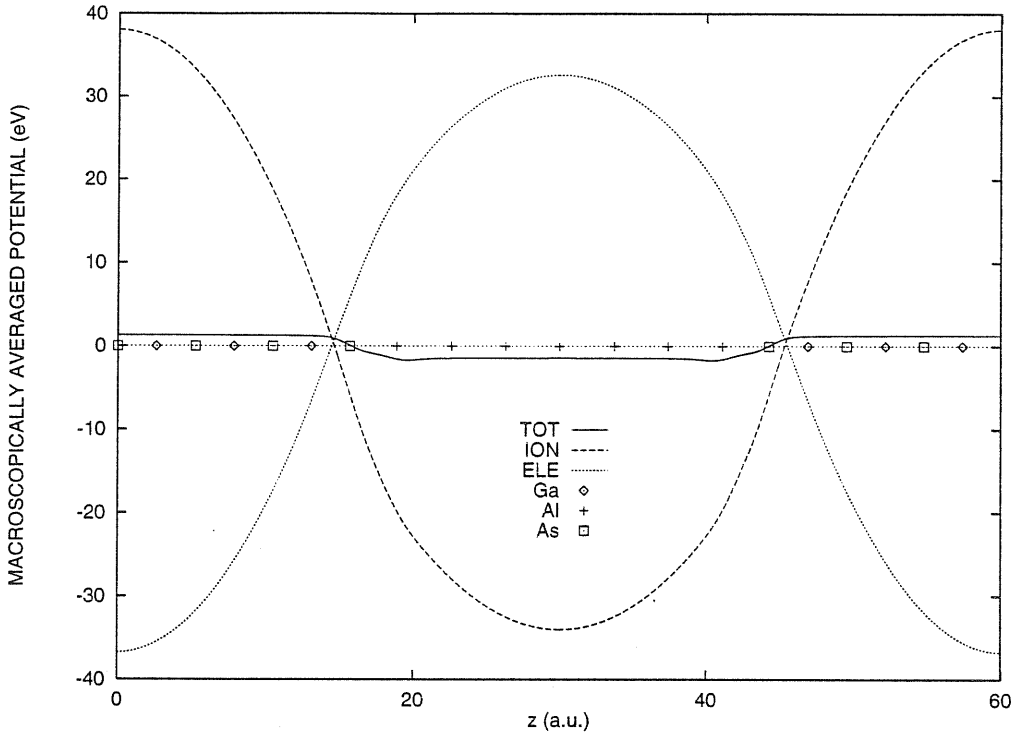

Figure 4.5: Macroscopic average of the electronic, ionic and total potential for the (001)Al/GaAs supercell.

charge tends to restore the unperturbed charge density of the bulk metal and of the bulk semiconductor up to a very short distance from the interface (we can therefore say that the interfacial region extend over less than about 6 Å); this behaviour is also evident by inspection of the macroscopically averaged electronic charge density (see Fig. 4.2).

The average of the electronic density in the semiconductor region is 8 electrons per primitive cell of bulk-GaAs (alias per GaAs linear period), while in the aluminum region—using our structural assumption—it corresponds to 8.485 electrons; these values are well reproduced by the selfconsistent charge in the supercell. We remind, by the way, that the one-dimensional period is of two planes in GaAs, while it is of one plane only in the Al region.

The ionic density in the semiconductor region requires 8 electrons per bilayer in order to satisfy the charge neutrality condition. But the last anion (As atom) is not compensated

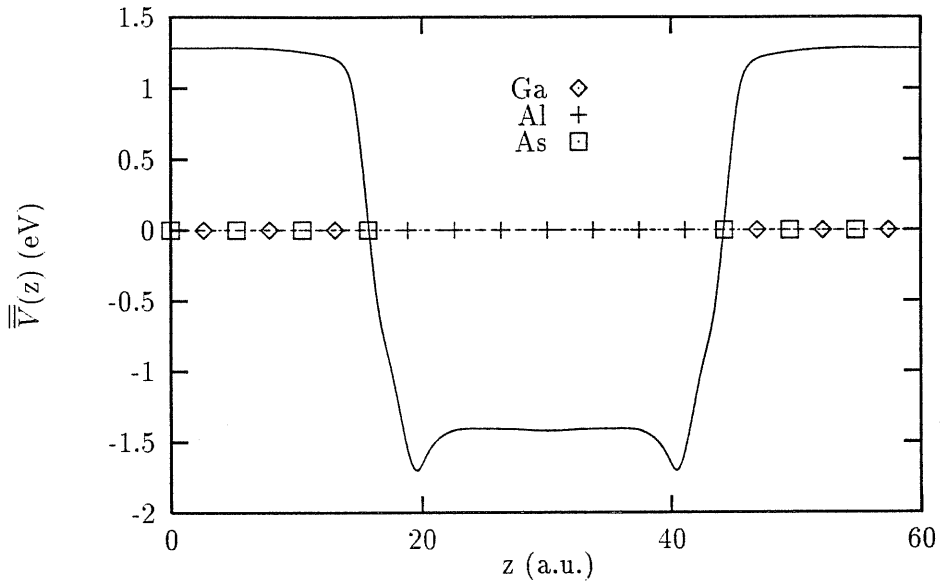

Figure 4.6: Macroscopic average of the total potential for the (001)Al/GaAs supercell.

and needs some extra electronic charge for satisfying the neutrality condition. This charge is provided by the metallic region, which acts as a reservoir. In fact, in Fig. 4.2 one sees a rather pronounced peak in the interfacial zone accounting for this effect.

The discontinuity of the average potential is the sum of two compensating terms, i.e. the Hartree potential and the ionic potential (see Fig. 4.5). The fact that their sum is nearly constant far from interface (as is evident from Fig. 4.6) assures *a posteriori* that the dimension of our supercell is sufficient. The global potential discontinuity that comes out is ΔV = 2.70 eV.

Therefore, we obtain a barrier height $\Phi_B^p = 0.78$ eV for (001)Al/GaAs junction, which turns out to be not perfectly in agreement with the experimental value. namely $\Phi_B^p = 0.66$ eV [18]. As emphasized above, however, we do not claim that our geometry is realistic.

The n-barrier calculation requires the knowledge of GaAs gap, which is not correctly provided by DFT method, because it is not a ground-state property. So we use the experimental value for the gap E_g (1.51 eV at 0K), and we obtain $\Phi_B^n = 0.73eV$ (the different experimental

values are around 0.80 eV).

4.3 Unperturbed (110)Al/GaAs junction

As in Section 3.2 we start our study of the (110)Al/GaAs junction using the fake aluminum which assures the lattice-matching condition with the GaAs substrate. In this condition, both ΔE_F and ΔE_v are unchanged with respect to the values obtained in the case of the unperturbed (001)Al/GaAs junction. So we have only to evaluate the discontinuity ΔV both of the Hartree potential and of the ionic one, in order to obtain the value of the SB-height. For this purpose we make use of the 7+7-supercell described in Section 2.2 and therefore we deal with 28 atoms.

As usually, it is important to check that the supercell is thick enough in order to reproduce bulk features in the region midway two adjacent interfaces: in particular problems could arise for the (110) oriented supercell, which is—for a given number of atoms—much shorter than the one in the (001) growth direction. Also in this case, we calculate the planar and macroscopic average both of the electronic (Figs. 4.7, 4.8) and of the ionic (Figs. 4.9, 4.10) charge density. As for the (001) case, the average number of electrons in the gallium arsenide region of the supercell per GaAs-periodicity must be 8, while in the aluminum region it corresponds to 8.485 electrons; it is seen that the actual result fluctuates a little bit around the expected value, thus demonstrating a slightly worse convergence in supercell size with respect to the other geometry studied so far. The outcoming potential discontinuity through the interface (see Fig. 4.11) turns out to be 2.58 eV: combining this result with ΔE_F and ΔE_v (obtained with bulk calculations), we gain for the SB height in the (110) direction Φ_B^p =0.90 eV. So, the difference with the (001) Φ_B^p is about 0.12 eV, which is beyond our computational error (that is estimated to be of the order of the hundredth of eV).

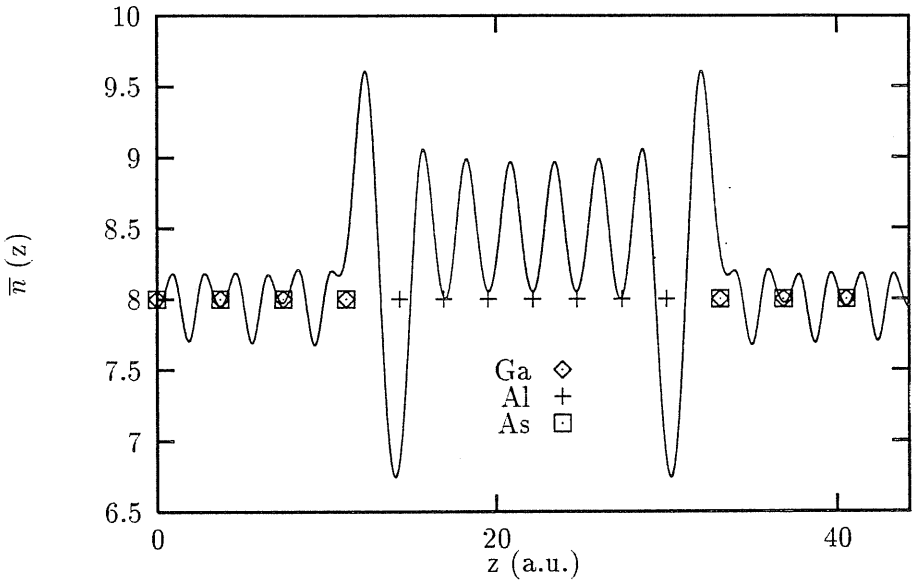

Figure 4.7: Planar average of the electronic charge density for the (110)Al/GaAs supercell.

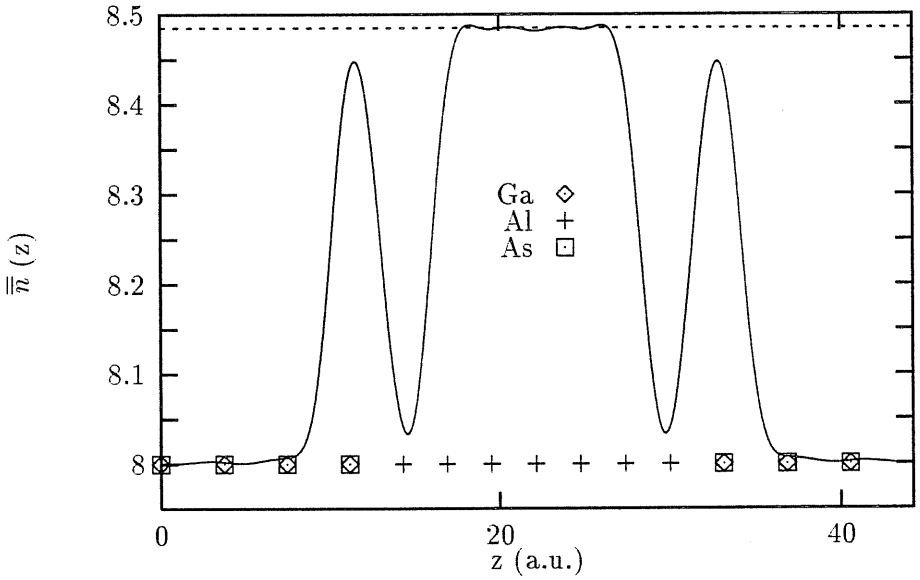

Figure 4.8: Macroscopic average of the electronic charge density for the (110)Al/GaAs supercell.

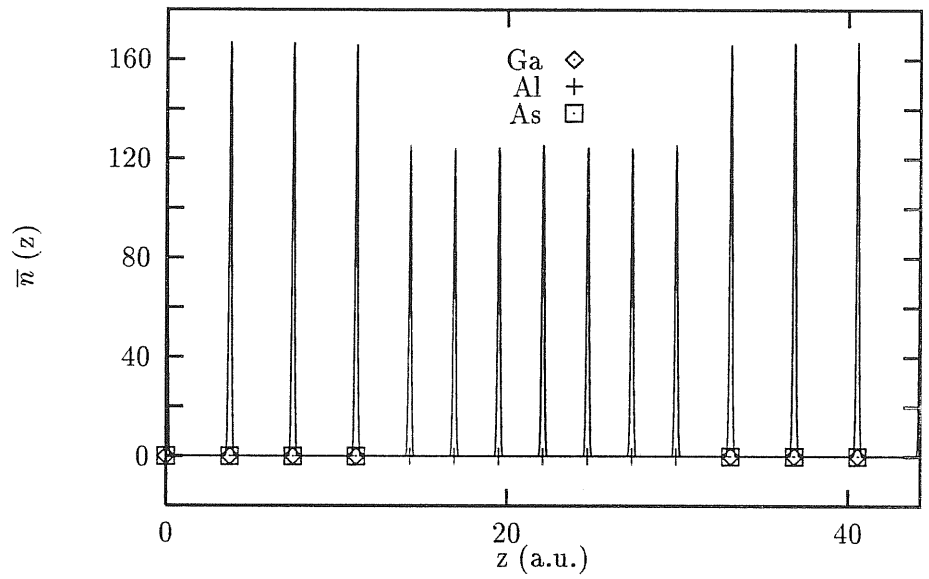

Figure 4.9: Planar average of the ionic charge density for the (110)Al/GaAs supercell.

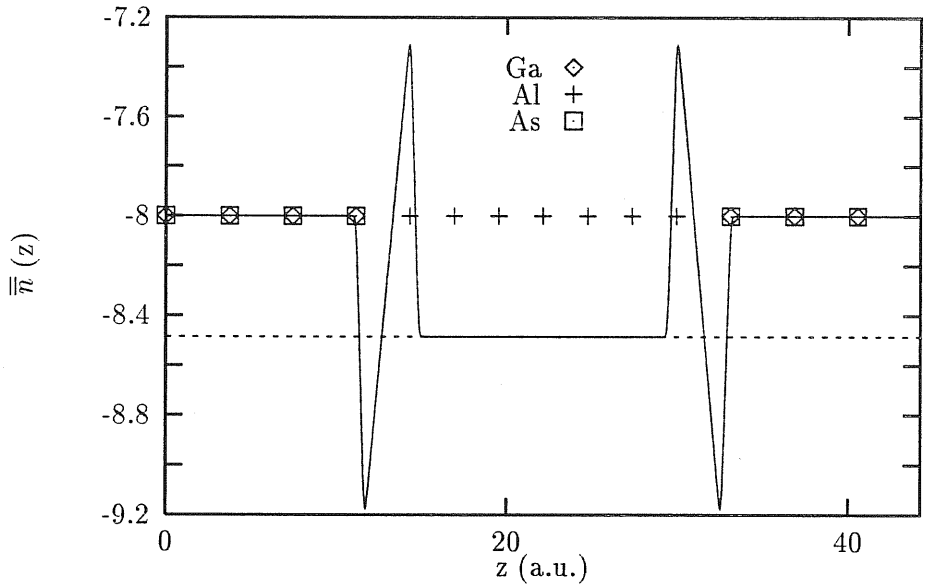

Figure 4.10: Macroscopic average of ionic charge density for the (110)Al/GaAs supercell.

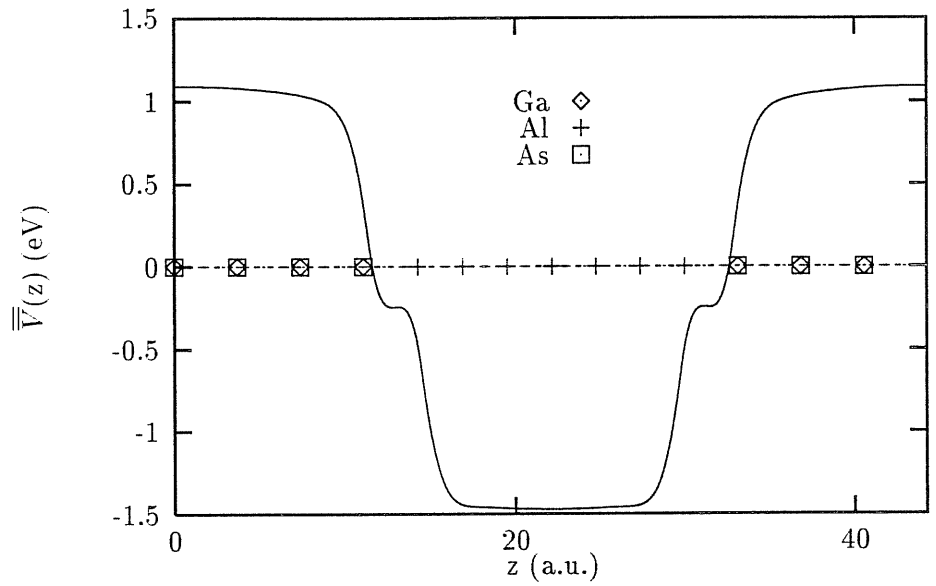

Figure 4.11: Macroscopic average of the total potential for the (110)Al/GaAs supercell.

4.4 Comparison with the (001)GaAs/vacuum interface

In order to gain a better understanding of the microscopic electronic structure of Al/GaAs interface, it might be useful to perform a study of GaAs/vacuum.

For the calculation of the potential line-up of the GaAs/vacuum interface we have utilized the supercell 13+7, already described in Section 2.2, where the Al atoms have been removed with no geometry relaxation of the remaining atoms. We study therefore an ideal unrelaxed As-terminated (001) surface. The study of the behaviour of the planar averaged charge density for the GaAs surface allows a comparison with a reference system and confirms that this charge peak means an effective charge transfer from the metal to the semiconductor at the level of last anion (see Fig 4.1 and Fig 4.12 for comparison). Furthermore, the charge profile of GaAs/vacuum interface shows that the GaAs charge density is recovered up to near the interface (see Figs. 4.12-4.13) as well as the bulk electrostatic potential (Fig. 4.14). The potential discontinuity through the interface is $\Delta V = 11.32$ eV and the presence of the vacuum region perturbs the semiconductor up to second anion. This calculation allows the

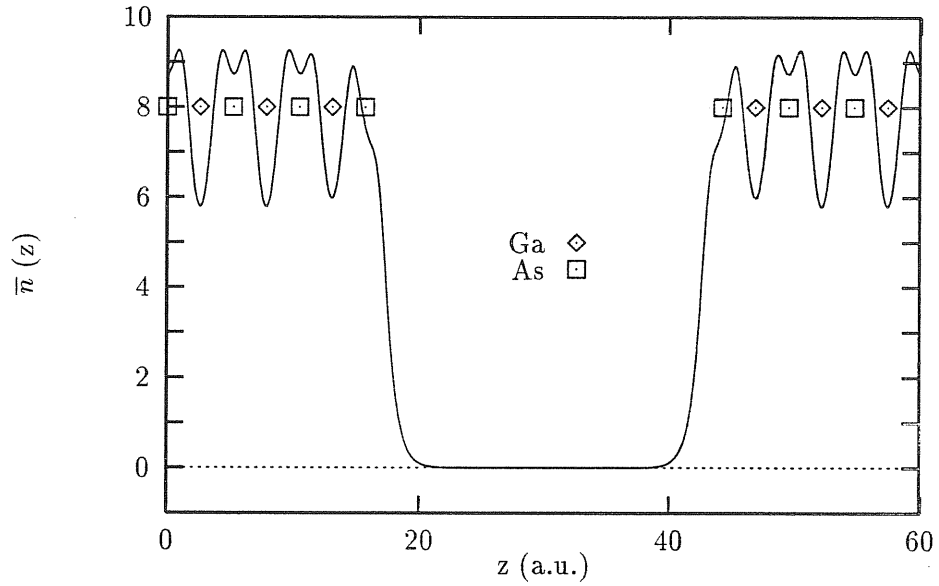

Figure 4.12: Planar average of the electronic charge density for the (001)GaAs/vacuum supercell.

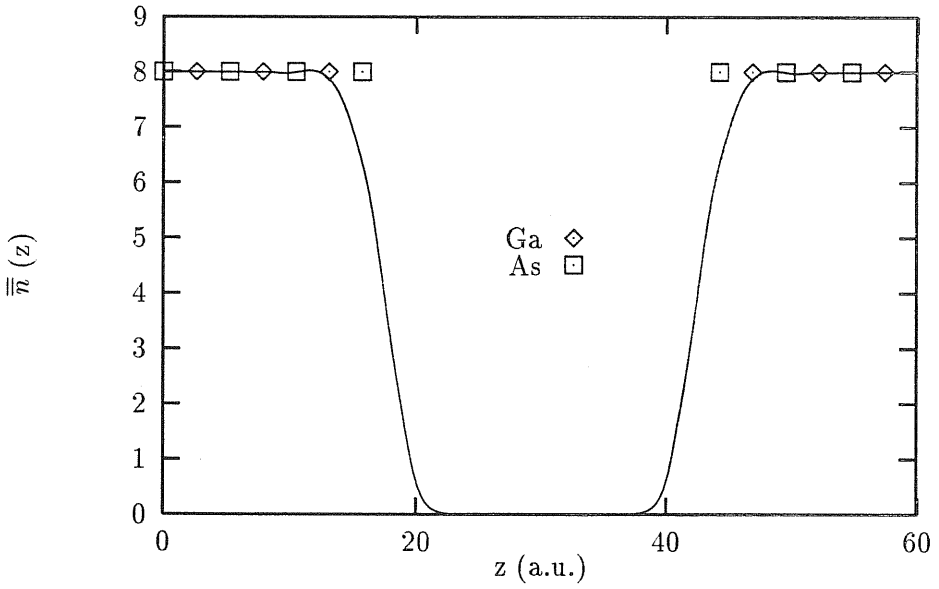

Figure 4.13: Macroscopic average of the electronic charge density for the (001)GaAs/vacuum supercell.

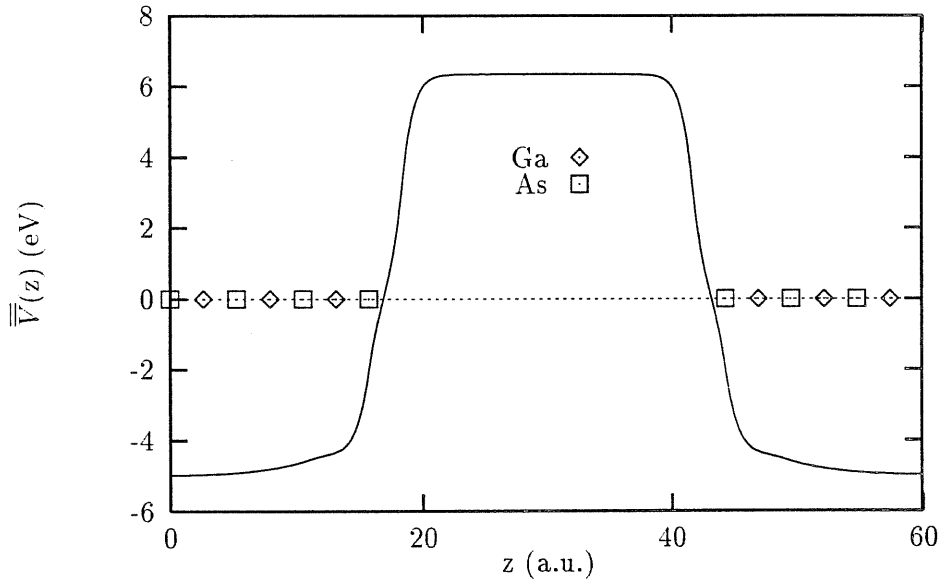

Figure 4.14: Macroscopic average of the total potential for the (001)GaAs/vacuum supercell.

evaluation of electron affinity χ_s of GaAs:

$$\chi_s = \Delta V - E_g - \Delta E_v, \tag{4.2}$$

then we obtain $\chi_s = 4.64$ eV for our ideal, unrelaxed and As-terminated (001) surface of GaAs. The measurement of the affinity is difficult and critically depends on surface reconstruction; the experimental values range from 4.7 to 5.1 eV [33].

4.5 Comparison with (001)Al/GaAs junction with some vacuum in between

The results of previous Section show that the potential discontinuity through the interface depends, as it is expected, from the fact that the metal is there. An interesting issue is how much the discontinuity depends on the *distance* between the metal and the semiconductor. According to the Schottky-Mott viewpoint, it should not depend at all. We want to check this prediction against a *quantitative* result.

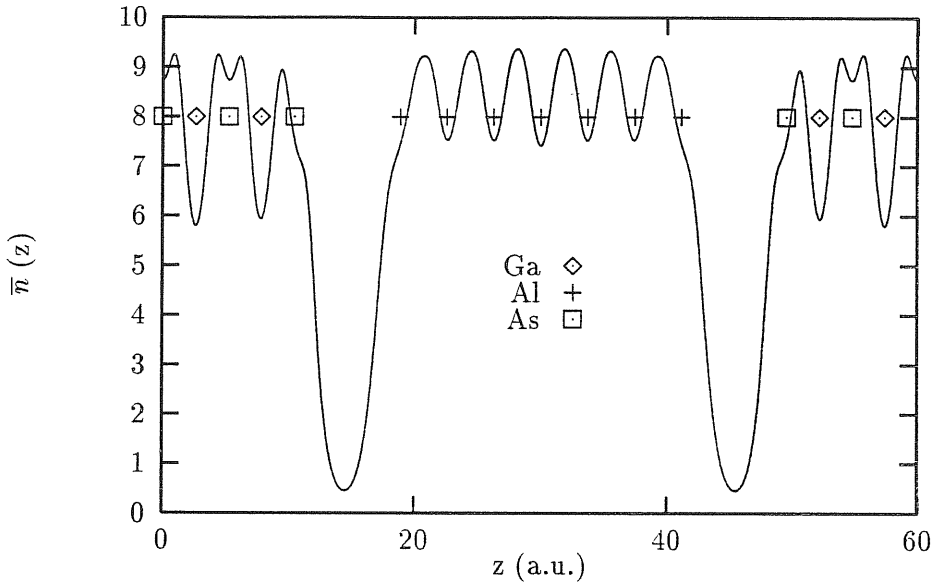

Figure 4.15: Planar average of the electronic charge density for the (001)Al/GaAs supercell without one bilayers of GaAs at each junction.

In order to investigate to which extent the metal-semiconductor distance affects the barrier, we thus performed some calculations by removing one bilayer of GaAs at each junction, without relaxing the positions of the remaining atoms (and so largely opening the Al-As bond). The planar and macroscopic average of the electronic charge are displayed respectively in Fig. 4.15 and in Fig. 4.16. The potential discontinuity one gets in this case displays, in effect, a huge difference with respect to the case when there is no vacuum between the semiconductor and the metal. This finding gives therefore further evidence (if any was needed) that the Schottky-Mott viewpoint is essentially incorrect, whereas instaed our calculations supports the hypothesis that the pinning effect is mostly a property of the Al-As bond.

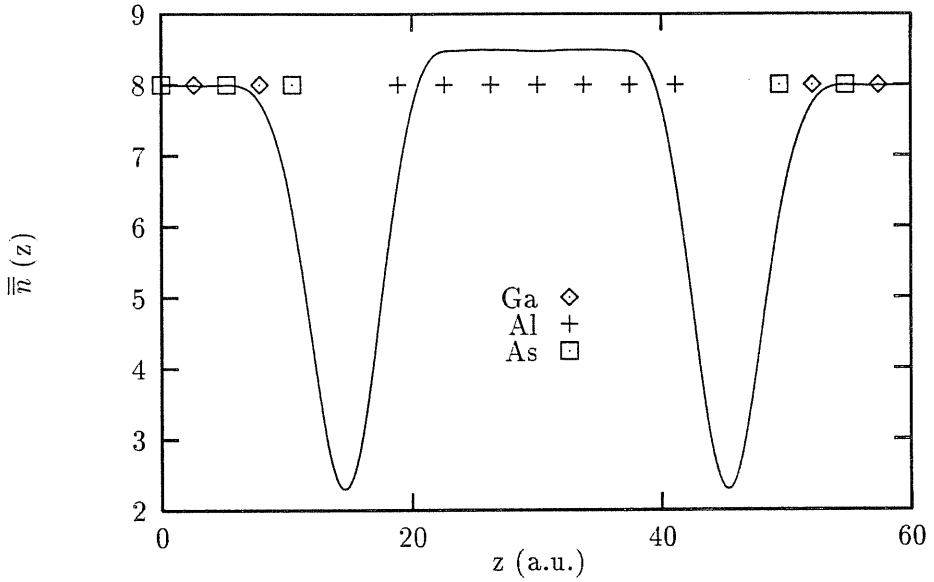

Figure 4.16: Macroscopic average of the electronic charge density for the (001)Al/GaAs supercell without one bilayer of GaAs at each junction.

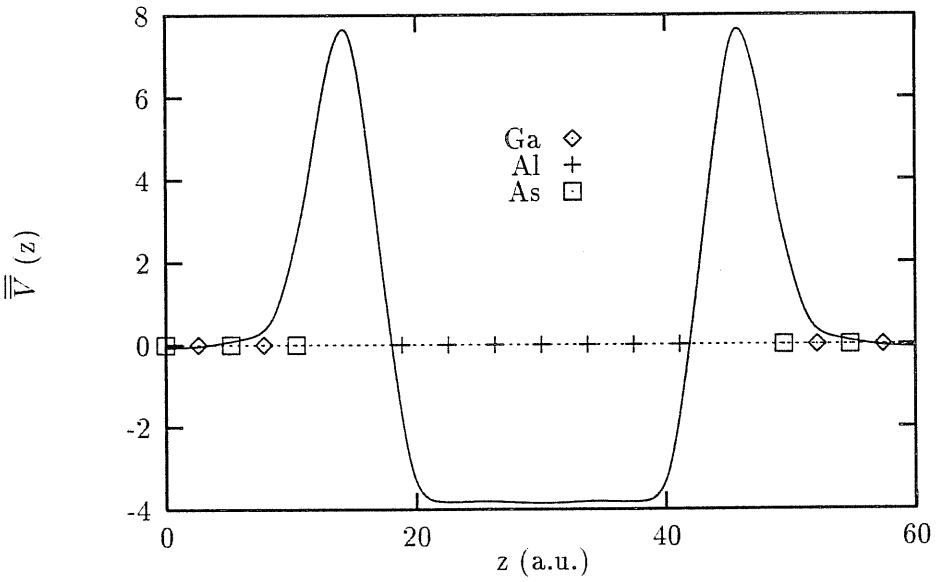

Figure 4.17: Macroscopic average of the total potential for the (001)Al/GaAs supercell without one bilayer of GaAs at each junction.

4.6 Transitivity rule

In order to check the transitivity relationships (2.2), we have performed the SB-height calculation also for (001)Al/AlAs and (110)Al/AlAs junctions.

As a preliminary step, we have carried out a convergence study of the equilibrium electronic and structural properties of AlAs (similar to the one done for GaAs and described in Section 3.1.1). We found that using plane waves up to kinetic energy $E_{cut} = 24$ eV and performing the BZ integration using a uniform (10×10×10) grid (i.e. 19 k-points), one obtain convergence within 1 mRy in the total energy and in the valence band top term, namely $\Delta E_v = 4.87$ eV, while the convergence conditions of structural parameters leads to a lattice constant $a_0 = 10.59$ a.u. and to a bulk modulus $B_0 = 75.2$ GPa.

With these informations, we are able to compute the SB height for both (001) and (110) directions for Al/AlAs junctions, following exactly the same procedure used for Al/GaAs case and using the same size of the supercells.

So, the SB height for the (001)-Al/AlAs junction turns out to be $\Phi_B^p = 1.19$ eV, while for the (110) case we gain $\Phi_B^p = 1.32$ eV.

Moreover, in order to verify the validity of Eq. 2.2, we performed the calculation of the valence band-offset for the GaAs/AlAs heterojunction and we obtained VBO = 0.42 eV.

The final results are summarized in tab. 4.3. In reading the table, one should bear in mind that we estimate our computational accuracy to be 0.01-0.02 eV. It is therefore evident that the transitivity relationship holds extremely well both for the (001) and for the (110) growth direction, while the two Schottky barrier are much different, well beyond our computational error.

Table 4.3: Transitivity relatioships for (001) and (110) interfaces among Al, GaAs and AlAs. In the first two columns are reported the calculated SB heights for Al/GaAs and Al/AlAs junctions, the third column reports their difference and the last one the value of calculated valence band-offset for AlAs/GaAs heterojunctions. All values are in eV.

direction	Al/AlAs	Al/GaAs	diff.	VBO (AlAs/GaAs)
(001)	1.17	0.74	0.43	0.42
(110)	1.33	0.92	0.41	0.41

4.7 Remarks, conclusions and future perspectives

Our calculation within DFT-LDA framework is in principle affected by few kinds of imprecisions, which however tend to compensate each other. First of all, the spin-orbit interaction removes the valence-band top degeneration at Γ point (causing a band splitting Δ=0.33eV) for GaAs. This effect decreases the p-barrier of $\sim$ 0.11eV. The many-body effects, beyond LDA, also modify the band terms and increase the p-barrier of about 0.1 eV. The relaxation of 3d electrons of GaAs plays a minor role. Needs *et alii* [2] showed that these three corrections compensate nearly perfectly (within about 0.01 eV).

Finally we can draw some conclusions from the work done: in particular we can make the assertion that the *pinning* exists and is an intrinsic property of the interface. It seems to depend crucially on the geometry of the Al-As bond. The model structure we have assumed, with the fake lattice-matched aluminum, allows us to neglect all irrelevant complications and to see rather clearly the phenomenon. Defects, even if certainly present, appear not to play a fundamental role in the barrier formation, because they are apparently not necessary for explaining the SB height behaviour. We also verified the validity of the transitivity rule for both (001) and (110) growth direction (which means that the difference between the

two kinds of barrier is an intrinsic property, which equals the VBO), even if the physical mechanism accounting for that is still to be identified.

As concerns perspectives for future work, our main purpose is to produce a more systematic collection of informations, in order to detect definitively which are the relevant features affecting the pinning mechanism.

In particular, as a first step in this direction, it could be interesting to separately study the effect of both macroscopic and microscopic strain on the Fermi level pinning.

Acknowledgments

I would like to express my gratitude to my supervisors, Prof. Raffaele Resta and Prof. Stefano Baroni, for introducing me in this new field of research and for their indispensable support and suggestions during the course of this work.

I am very grateful to Dr. Stefano de Gironcoli, who always responded with the utmost patience to all my questions, even the most elementary ones, and to Dr. Claudia Bungaro, whose availability in helping (both from a scientific and from a human point of view) is really unlimited!

I want to thank also all my friends here in SISSA, and in particular (in strict alphabetic order!) Barbara, Carlo, Claudio, Daniele, Giovanni, Lorenzo, Marco, Orion and many more, for their help and especially for their true friendship.

Finally, I thank all the people who have been always close to me with their encouragements and their love: my parents, my brothers, Andrea and all my friends.

Bibliography

[1] S. B. Zhang, Marvin. L. Cohen, and Steven G. Louie, Phys. Rev. B **34**, 768 (1986).

[2] R. J. Needs, J. P. A. Charlesworth and R. W. Godby, Europhys. Letters **25**, 31 (1994).

[3] R. G. Dandrea and C.B. Duke, J. Vac. Sci. Technol. B **11**, 848 (1993); ibid. 1553.

[4] J. Bardi, *Barriere de Schottky des Jonctions* $Al/Ga_{1-x}As_x$, Travail Pratique de Diplôme d'Ingénieur Physicien EPFL, École Polytechnique Fédérale de Lausanne (1995).

[5] B. L. Sharma, *Metal-Semiconductor Schottky Barrier Junctions and their Applications*, Plenum, New York (1984).

[6] F. Capasso and G. Margaritondo, *Heterojunction Band Discontinuity: Physics and Device Applications*, North-Holland, Amsterdam (1987).

[7] W. Mönch, *Electronic Structure of Metal-Semiconductor contacts*, Jaca Book, Milano (1990).

[8] N. F. Mott, Proc. Cambridge Philos. Soc., **34**, 568 (1938).

[9] J. Bardeen, Phys. Rev. **71**, 717 (1947).

[10] V. Heine, Phys. Rev. A **138**, 1689 (1965).

[11] H. H. Wieder, J. Vac. Sci. Technol. **15**, 1498 (1978).

[12] W. E. Spicer, P. W. Chye, P. R. Skeath and I. Lindau, J. Vac. Sci. Technol. **16**, 1422 (1979).

[13] J. L. Freeouf and J. M. Woodall, Appl. Phys. Lett. **39**, 727 (1986).

[14] C. B. Duke and C. Mailhot, J. Vac. Sci. Tech. B **3**, 1170 (1985).

[15] W. A. Harrison, J. Vac. Sci. Tech. B **3**, 1231 (1985).

[16] J. Tersoff, Phys. Rev. Lett. **52**, 6 (1984); J. Tersoff, Phys. Rev. B **30**, 8 (1984).

[17] R. Ludeke, and G. Landgren, J. Vac. Sci. Technol. **19**, 667 (1981).

[18] P. Revva, J. M. Langer, M. Missous and A. R. Peaker, J. Appl. Phys. **74**, 416 (1993).

[19] L. Dobaczewski, J. M. Langer and M. Missous, Acta Physica Polonica A **84**, 741 (1993).

[20] P. Hohemberg and W. Kohn, Phys. Rev. **136**, B864 (1964).

[21] W. Kohn and J. L. Sham, Pys. Rev. **140**, A1133 (1965).

[22] G.B. Bachelet, D.R. Hamann and M. Schlüter, Phys. Rev. B **26**, 4199 (1982).

[23] N. Troullier and J. L. Martin, Phys. Rev. B **43**, 1993 (1991).

[24] G.B. Bachelet and N.C. Christensen, Phys. Rev. B **8**, 5747 (1973).

[25] W.E. Pickett, Comp. Phys. Rep. **9**, 115 (1989).

[26] S. Baroni, R. Resta, A. Baldereschi, and M. Peressi, in *Spectroscopy of Semiconductor Microstructures*, edited by G. Fasol, A. Fasolino, and P. Lugli, NATO ASI Ser. B, Vol. 206 (Plenum, NY, 1989), p.251.

[27] A. Baldereschi, S. Baroni, and R. Resta, Phys. Rev. Lett. **61**, 734 (1988).

[28] H. J. Monkhorst and J.D. Pack, Phys. Rev. B **13**, 5188 (1976).

[29] L. Kleinman, and D.M. Bylander, Phys. Rev. Lett. **48**, 1425 (1982).

[30] X. Gonze, P. Käckell, and M. Scheffler Phys. Rev. B **41**, 12264 (1990).

[31] U. von Barth and R. Car (unpublished).

[32] M. Methfessel, and A.T. Paxton, Phys. Rev. B **40**, 3616 (1989).

[33] J. Massies, P. Devoldere and N. T. Linh, J. Vac. Sci Thecnol. **16**, 5 (1979).